Online Methods

Clinical Tissue sample collection

Tubercular human lung tissue was removed during therapeutic lung resection surgery at the National Masan Hospital (NMH) from participants infected with multi-drug resistant tuberculosis and refractory to second-line drug therapy. Tissue collection for the study of "*M. tuberculosis* acquired drug resistance distribution in the human lung" had been described previously[41], and was approved by the NMH institutional review board, an exemption from NIH, and with written consent of the subjects; samples collected between 2002 and 2008 were de-identified when provided for dissection. Tissues used in this study were from a set of six consecutive participants with tissues samples displaying the three types of pathological structures analyzed (**Supplemental Table 1**). The participants (2006-2008) were 19 to 45 years (median 28 years), HIV-negative, and had received TB treatment for 6 to 36 months (average 17 months). The *M. tub*erculosis isolates were resistant to 3 to 8 (median 5) anti-TB agents including isoniazid, rifampin, streptomycin, ofloxacin, pyrazinamide and kanamycin. The resected lung was immediately transferred to Biological safety Class II cabinet and dissected into regions of normal and affected lung, the lesions were separated and fixed in 10 % neutral buffered Formalin for at least 24h, dehydrated and paraffin embedded. Section from each block were prepared for Hematoxylin and Eosin staining and the stained slides were imaged at 20X using an Aperio CS2 image capture device (Leica Biosystems, Buffalo Grove IL, USA) and images were reviewed by an experienced pathologist. A summary of patient and tissue details are in Supplemental Table 1A.

Rabbit infection and lesion dissection

Animal studies were carried out in accordance with the Guide for the Care and Use of Laboratory Animals of the National Institutes of Health, with approval from the

Institutional Animal Care and Use Committee of the New Jersey Medical School, Newark, NJ. Specific pathogen-free, individually housed female NZW rabbits, weighing 2.2 to 2.6 kg, were used for aerosol infection by *M. tuberculosis* HN878, as previously described[42], since it generates a representative range of human-like lesions in infected rabbits. Briefly, rabbits were exposed to *M. tuberculosis*-containing aerosol using a nose-only delivery system. Three hours post-infection, rabbits were euthanized, and serial dilutions of the lung homogenates were cultured on Middlebrook 7H11 agar plates to enumerate the number of bacterial colony forming units (CFUs) implanted in the lungs. The infection was allowed to progress for 16 to 20 weeks, at which point the animal were euthanized to dissect lesions as previously described[36]. The four lesions analyzed in this study, two cellular and two caseous granulomas, originate from three rabbits and were randomly selected from a large bank of archived lesions (**Supplemental Table 1**). They represent the most common lesion types seen in rabbits with chronic active TB, as observed through numerous studies performed by our group with large rabbit cohorts.

Proteomic analysis

To obtain histologically distinct compartments, tuberculous lung tissue was dissected to five separate granuloma regions with the Laser Pressure Catapulting (LPC) PALM Instrument (Zeiss, Göttingen, Germany). Collected tissue samples were lysed in a buffer consisting of 0.1 M Tris–HCl, pH 8.0, 0.1 M DTT, and 4% SDS at 99 °C as described earlier[43]. Lysates were loaded on ready-made gel (NuPage 10% Bis-Tris, Invitrogen) and run to only an inch of separation using gel electrophoresis. The samples were then subjected to in-gel digestion (LysC and trypsin) and peptide extraction with StageTips as described previously[44].

LC-MS/MS analysis of resulting peptides was performed as single-shot runs[45], using Q-Exactive mass spectrometer[46] (Thermo Fisher Scientific) coupled on-line to a nanoflow UHPLC instrument (Easy nLC, Thermo Fisher Scientific). Chromatographic

peptide separation was done over a 240 min gradient on a reverse phase 50 cm long column. For measurements using Q Exactive mass spectrometer, a resolution of 70,000 at m/z 400 was used for survey scans and up to 10 dynamically chosen most abundant precursor ions were fragmented (isolation window 1.6 m/z). The survey scans (300–1700 m/z, target value 3E6, maximum ion injection times 20 ms) were acquired and followed by higher-energy collisional dissociation (HCD) based fragmentation (normalized collision energy 25). The MS/MS scans were acquired at a resolution of 17,000 at m/z 400 (target value 1E6, maximum ion injection times 60ms).

Mass spectra were analyzed using MaxQuant computational platform version 1.3.0.5 and Andromeda[47] against the Uniprot FASTA human database. The search included cysteine carbamidomethylation as a fixed modification and N-acetylation of protein and oxidation of methionine as variable modifications. A false discovery rate (FDR) of less than 0.01 for proteins and peptides and a minimum peptide length of 7 amino acids were required. Proteome quantification was performed in MaxQuant using the XIC based inbuilt label-free quantification (LFQ) algorithm[37]. Label free intensities were logarithmized and empty values were imputed with random numbers from a normal distribution, whose mean and standard deviation were chosen to best simulate low abundance values close to noise level.

The mass spectrometry proteomics data have been deposited to the ProteomeXchange Consortium (http://proteomecentral.proteomexchange.org) via the PRIDE partner repository with the dataset identifier PXD003646.

Bioinformatic analyses were performed in the Perseus software environment. Pathway membership information was obtained from KEGG pathways and categorical annotation was supplied as GO biological process (BP), molecular function (MF), and cellular component (CC). We filtered for protein groups that were accurately quantified in at least two granuloma regions and showed at least 1.5-fold differential expression

between at least two granuloma regions. Unsupervised hierarchical clustering was performed after z-score normalization of the regulated dataset. PCA was performed on the quantified proteins and we tested for enrichment of annotation categories in individual PCA components. We tested and computed the difference between medians of the two groups – proteins corresponding to an annotation category versus all proteins in the dataset. We did this for every annotation term using two-sided Wilcoxon-Mann-Whitney test where the multiple hypothesis testing is adjusted by applying a Benjamini-Hochberg FDR threshold of 0.05. For significant annotation terms, a 'difference' is reported, indicating where the center of the distribution for the annotation category is located relative to the overall distribution. We used this approach to identify significantly different annotation terms in principal component one that separates the caseum from the cellular periphery and report their 'difference' and *P*-values for GO annotation terms and KEGG pathways.

Immunohistochemistry

A summary of clinical and rabbit tissue samples utilized for IHC studies are included in Supplemental Table 1C and 1D. Paraffin lung tissue sections were cut at 10 to 20 µm thickness, mounted on ultraclean glass slides covered in silane, deparaffinized, then dehydrated and rehydrated using the following steps: Ethanol solutions (30, 50, 70, 90, 95 and 100 % for 3 min each), xylenes (2 different solutions for 10 min each) and ethanol solutions (100, 95, 90, 70, 50 and 30 for 3 min each). The slides were washed once in Tris buffer Saline (TBS) for 5 min. Slices were subjected to antigen retrieval by boiling in sodium citrate buffer at pH=6.0 for 20 min and incubated in Triton-X 0.1% for 5 min. Slices were removed and allowed to equilibrate to room temperature for at least 20 min, and rinsed with distilled water.

Tissue sections were blocked (blocking solution; 0.5 M EDTA, 1% horse serum,

1% Ig free BSA, 4% human serum, and 1% fish gelatin in PBS) and incubated overnight in primary antibodies against the proteins related to our studies (see **Supplemental Table 6**). After incubation, the tissues were washed several times with sterile TBS at room temperature and incubated in the respective secondary antibodies (anti-mouse, anti-goat or anti-rabbit conjugated to Alexa-488, Alexa588, or Alexa-647) and streptavidin conjugated to Texas-red for mycobacterium detection for at least 1h at room temperature. Tissue sections were mounted using Prolong Gold Antifade reagent (Invitrogen, grand Island, NY) with DAPI, and the tissue sections were examined in an A1 confocal microscope equipped with a spectrum detection and unmixing systems (Nikon Instruments Inc, Japan). Antibody specificity was confirmed by replacing the primary antibody with a non-specific myeloma protein of the same isotype or non-immune serum.

Three-dimensional reconstruction and deconvolution of areas of interest was performed from 12 to 25 optical sections obtained at 0.250 or 0.150 μm intervals[48]. To analyze and quantify abundance of the study proteins, the number of positive pixels as well as their intensity in macrophages were measured in specific regions of interest. In addition, for each cell population, a linear intensity histogram was generated to examine the expression of each enzyme inside defined cell types or in caseum. By using this approach, we identified up to 8 different compartments represented in cellular, necrotic and cavitary granulomas. These compartments included caseum, macrophage processes towards the caseum, macrophage cell bodies, fibrotic areas, areas outside of the inflammatory ring, normal tissue, clusters of inflammatory cell within the normal tissue, and multinucleated giant cells. To compare protein abundance across tissues, similar numbers of cells and areas were included in the 3D deconvoluted optical reconstructions. This analysis avoids problems associated with inflammatory versus normal tissues where density and structure of the tissue are different.

Adjacent sections were stained with hematoxylin & eosine, and trichrome Masson to correlate the confocal findings with histopathology as well as with MALDI mass spectrometry imaging (MSI) of the same tissue sections.

Tissue sectioning and matrix application

Twelve μm thick tissue serial sections were prepared using a Leica CM1850 cryostat (Buffalo Grove, IL) and thaw-mounted onto stainless steel slides (for MALDI-MSI analysis) or frosted glass microscope slides (for H&E staining). After sectioning, tissues were allowed to dry at room temperature for 15 minutes and then transferred to a -80°C freezer for storage.

Prior to MALDI-MSI analysis, tissue sections were removed from the -80 °C freezer and allowed to reach room temperature for 15 minutes. A number of matrices were evaluated for lipid imaging. α-Cyano-4-hydroxycinnamic acid (CHCA), 2,5-dihydroxybenzoic acid (DHB), and 9-Aminoacridine (9-AA) were purchased from Sigma Aldrich (St Louis, MO). Matrices for MALDI MSI analysis were optimized for each imaging mode, shown in Supplemental Table 4.

MALDI-MSI Analysis

MALDI-MSI analysis was performed using a MALDI LTQ Orbitrap XL mass spectrometer (Thermo Fisher Scientific, Bremen, Germany) with a resolution of 100,000 at *m/z* 400, full width half maximum (FWHM). External mass calibration was performed using Proteomass™ mass calibration kit (Sigma Aldrich, St Louis, MO). Lipids were initially identified by their exact mass and the identities confirmed by performing MS/MS analysis of intact precursor ions direct from adjacent tissue sections. Accurate mass-measured lipid peaks were identified as phospholipids, lysophospholipids and free fatty acids by matching to reference lipids in the LIPID MAPS and Human Metabolome

Database within a ±0.002 Da mass tolerance window. Collision induced dissociation was performed on lipid precursor ions with a mass window of 2 Da. Identified lipids along with their precursor and identifying fragment masses are shown in **Supplemental Table 5**. Fragmentation patterns were manually interpreted to confirm lipid identities.

For positive mode imaging analysis, a laser intensity of 5 µJ was applied and 20 laser shots were fired at each position (total of 1 microscan per position). The laser step size was set to 75 µm. For negative mode analysis, a laser intensity of 7 µJ was used and 25 shots were fired at each position (total of 1 microscan per position). The laser step size was set to 75µm.

Data visualization was performed using Thermo ImageQuest software. Ion images were plotted within a ±0.002 *m/z* mass tolerance window and all lipid images were normalized to the total ion current (TIC) chromatogram. Extracted ion images were interpolated using the linear interpolate function.

Lipid quantification

Sample collection and processing: Tissue samples were weighed and homogenized in 4 volumes of phosphate buffered saline (PBS). Homogenization was achieved using a FastPrep-24 instrument (MP Biomedicals) and 1.4 mm zirconium oxide beads (Precellys). Proteins were precipitated by adding 9 volumes of methanol with 1% formic acid to 1 volume of plasma or homogenized tissue sample. The mixtures were vortexed for 2min and centrifuged at 4,000 rpm for 5 min. The supernatant was dried down and reconstitute in 40 uL of 30% MeOH, prior to LC/MS-MS analysis.

High pressure liquid chromatography coupled to tandem mass spectrometry (LC/MS-MS) analytical methods: 6k-$PGF_{1\alpha}$ quantification was performed at VCU Lipidomics Core Facility[49]. Briefly, reconstituted tissue extracts were analyzed via HPLC

ESI-MS/MS. A 30 min reversed-phase LC method utilizing a Kinetex C18 column (100 × 2.1 mm, 2.6 µm) was used to separate the eicosanoids at a flow rate of 200 µl/min at 50 °C. The column was equilibrated with 100% Solvent A [acetonitrile:water:formic acid (40:60:0.02, v/v/v)] for 5 min and then 10 µl of sample was injected. 100% Solvent A was used for the first minute of elution. Solvent B [acetonitrile:isopropanol (50:50, v/v)] was increased in a linear gradient to 25% Solvent B to 3 min, to 45% until 11 min, to 60% until 13 min, to 75% until 18 min, and to 100% until 20 min. 100% Solvent B was held until 25 min, then was decreased to 0% in a linear gradient until 26 min, and then held until 30 min. The eicosanoids were then analyzed using a tandem quadrupole mass spectrometer (ABI 4000 Q-Trap®, Applied Biosystems) via multiple reaction monitoring (MRM) in negative-ion mode. The specific MRM transition monitored for 6k-$PGF_{1\alpha}$ and the internal standard (6k-$PGF_{1\alpha}d_4$) were *m/z* 369→163 and *m/z* 373→167 respectively. The mass spectrometer parameters used were: curtain gas, 30; CAD, high; ion spray voltage, −3,500 V; temperature, 500°C; gas 1, 40; gas 2, 60; declustering potential, collision energy, and cell exit potential were optimized per transition.

Methods-only references

36. Prideaux, B. *et al.* The association between sterilizing activity and drug distribution into tuberculosis lesions. *Nat. Med.* **21,** 1223–1227 (2015).
37. Cox, J. *et al.* Accurate proteome-wide label-free quantification by delayed normalization and maximal peptide ratio extraction, termed MaxLFQ. *Mol. Cell Proteomics* **13,** 2513–2526 (2014).41. Leong, F., Eum, S. & Via, L. E. Pathology of tuberculosis in the human lung. *… Pulmonary Tuberculosis* (2011).
42. Subbian, S. *et al.* Chronic pulmonary cavitary tuberculosis in rabbits: a failed host immune response. *Open Biol* **1,** 110016–110016 (2011).
43. Ostasiewicz, P., Zielinska, D. F., Mann, M. & Wiśniewski, J. R. Proteome, phosphoproteome, and N-glycoproteome are quantitatively preserved in formalin-fixed paraffin-embedded tissue and analyzable by high-resolution mass spectrometry. *J. Proteome Res.* **9,** 3688–3700 (2010).
44. Sharma, K. *et al.* Quantitative analysis of kinase-proximal signaling in lipopolysaccharide-induced innate immune response. *J. Proteome Res.* **9,** 2539–2549 (2010).
45. D'Souza, R. C. J. *et al.* Time-resolved dissection of early phosphoproteome and ensuing proteome changes in response to TGF-β. *Sci Signal* **7,** rs5–rs5 (2014).

46. Michalski, A. *et al.* Mass spectrometry-based proteomics using Q Exactive, a high-performance benchtop quadrupole Orbitrap mass spectrometer. *Mol. Cell Proteomics* **10,** M111.011015–M111.011015 (2011).
47. Cox, J. *et al.* Andromeda: a peptide search engine integrated into the MaxQuant environment. *J. Proteome Res.* **10,** 1794–1805 (2011).
48. Guan, Y. Q., Cai, Y. Y., Zhang, X., Lee, Y. T. & Opas, M. Adaptive correction technique for 3D reconstruction of fluorescence microscopy images. *Microsc. Res. Tech.* **71,** 146–157 (2008).
49. Mietla, J. A. *et al.* Characterization of eicosanoid synthesis in a genetic ablation model of ceramide kinase. *J. Lipid Res.* **54,** 1834–1847 (2013).

Supplemental figures and Tables:

Supplemental Figure 1:

(**a**) Lung images showing granuloma regions that were dissected by Laser-Capture Microdissection. These included the interior of a solid granuloma, the cellular borders of the caseous and cavitary granulomas, as well as the necrotic caseum of the caseous and cavitary granulomas. (**b**) A bar chart showing number of proteins identified by a single-run analysis of the indicated granuloma caseum or cells with FDR of 1%.

Supplemental Figure 2:

(**a**) Clustering analysis and heat map of protein intensities for the 5 sample types. (**b**) A bar chart showing number of proteins quantified and proteins not quantified. Fewer proteins were identified and quantified in 'Caseous Granuloma, Cells' sample; in contrast with other 4 samples, we obtained quantitative information for less than half of the identified proteins in this sample. (**c**) List of proteins that were enriched in necrotic regions of the caseous and cavitary granulomas.

Supplemental Figure 3:

(**a**) AA is released from membrane phospholipids by multiple phospholipases. (**b**)

Proteomic profiling of phospholipases. AA-releasing phospholipases (PLA) are diffusely expressed. AA-depleting acyl-transferases (MBOAT) show the opposite pattern. (**c**) IHC of secreted phospholipases (left) and matching H&E (right). Secreted phospholipases, $sPLA_2$-II, $sPLA_2$-V, $sPLA_2$-X (green fluorescence) are diffusely expressed in both caseous and cavitary granulomas.

Supplemental Figure 4:

LTA4H is enriched at the caseum border in both caseous and cavitary granulomas. H&E (upper left) and IHC for LTA4H in caseous granuloma (left) and in cavitary granuloma (right) in green fluorescence, DAPI (blue) and IBA1 (cyan).

Supplemental Figure 5: (**a**) IHC staining showing similar localization of TNF-α and LTA4H in caseous regions of the cavitary granulomas. IHC staining for TNF-α (red), LTA4H (green), nuclei using DAPI (blue), and macrophages using IBA1 (cyan). (**b**) IHC staining of TNF-α (red), LTA4H (green), nuclei using DAPI (blue), and macrophages using IBA1 (cyan) in one representative rabbit granuloma (n=4). TNF-α and LTA4H showed similar patterns of distribution in all 4 lesions studied.

Supplemental Figure 6:

(**a**) Example granulomas with borders around dissected regions. (**b**) COX1 and COX2 are diffusely expressed in cavitary granulomas. H&E (upper left) and IHC for COX1 (left) and COX2 (right) in green fluorescence, DAPI (blue) and IBA1 (cyan). (**c, d**) IHC staining of TNF-α (red), LTA4H or COX2 (green), nuclei using DAPI (blue), and macrophages using IBA1 (cyan) of rabbit lesions.

Supplemental Table 1:

(**a**) Summary of patient details and clinical samples utilized in the study. (**b**) Clinical samples used for laser capture microdissection (LCM) and proteomics. (**c**) Details of clinical tissue samples utilized for MALDI-MSI and immunohistochemistry (IHC). (**d**) Details of rabbit lesions used for MALDI-MSI and IHC.

Supplemental Table 2:

Excel file of the raw data of all the proteomes; interior of a solid granuloma, the cellular borders of the caseous and cavitary granulomas, as well as the necrotic caseum of the caseous and cavitary granulomas. This includes imputed values as a separate sheet.

Supplemental Table 3:

PCA GO and KEGG enrichment table

Supplemental Table 4. Matrix systems used to analyze lipids in pulmonary lesion biopsies. All matrices were applied to the tissue by airspray deposition. The airbrush (Paasche Model VL, Chicago, IL) was positioned at a distance of 30cm from the tissue and 20 passes over the tissue were performed with the tissue being allowed to dry for 30 seconds between coatings.

Supplemental Table 5. List of glycerophospholipid species as identified by accurate mass MALDI and MS/MS direct from tissue

Supplemental Table 6:

Details of IHC antibodies used for human and rabbit tissues in this study.

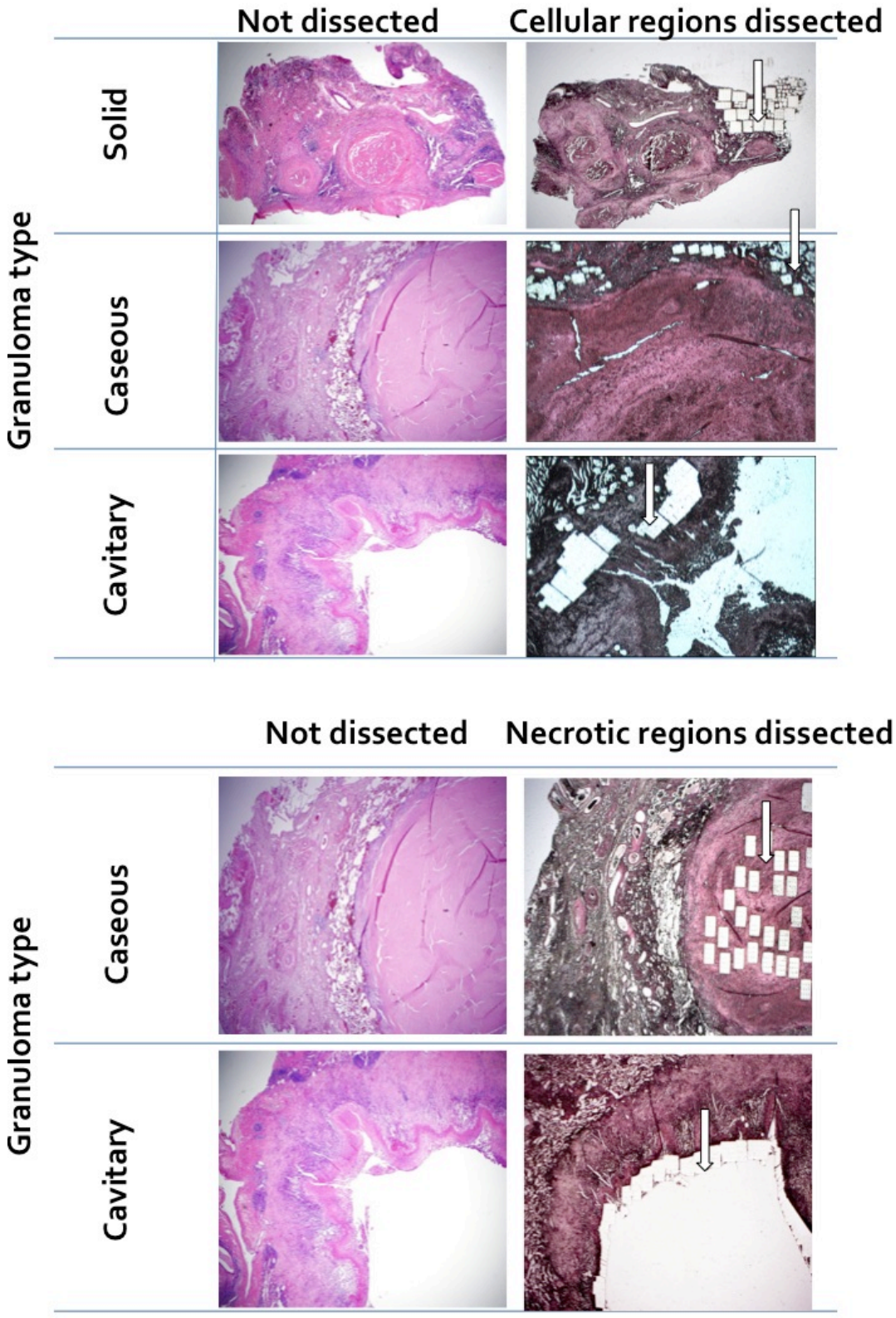

Supplemental Figure 1A

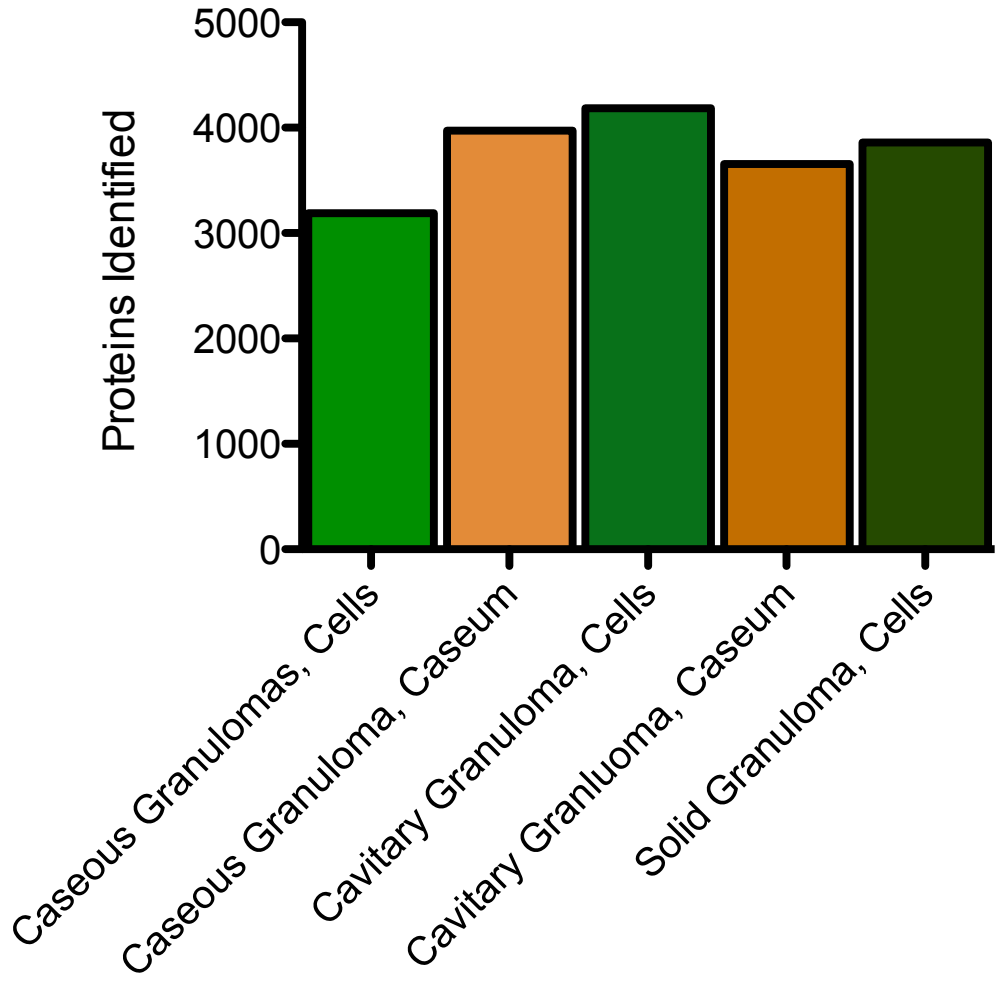

Supplemental Figure 1B

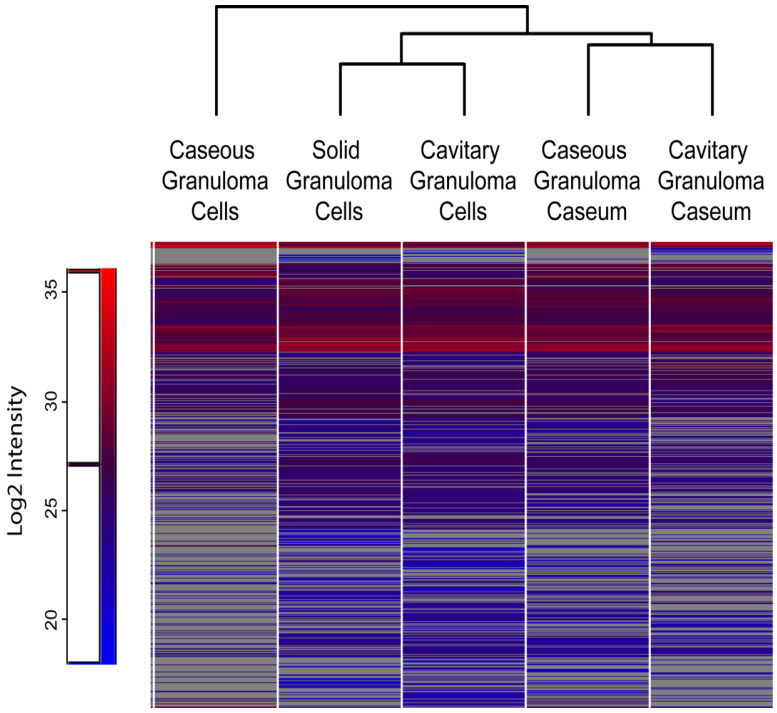

Supplemental Figure 2A

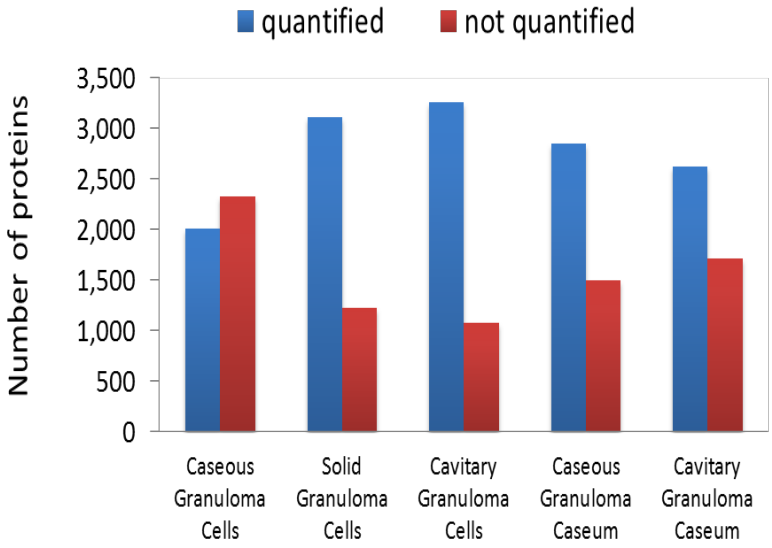

Supplemental Figure 2B

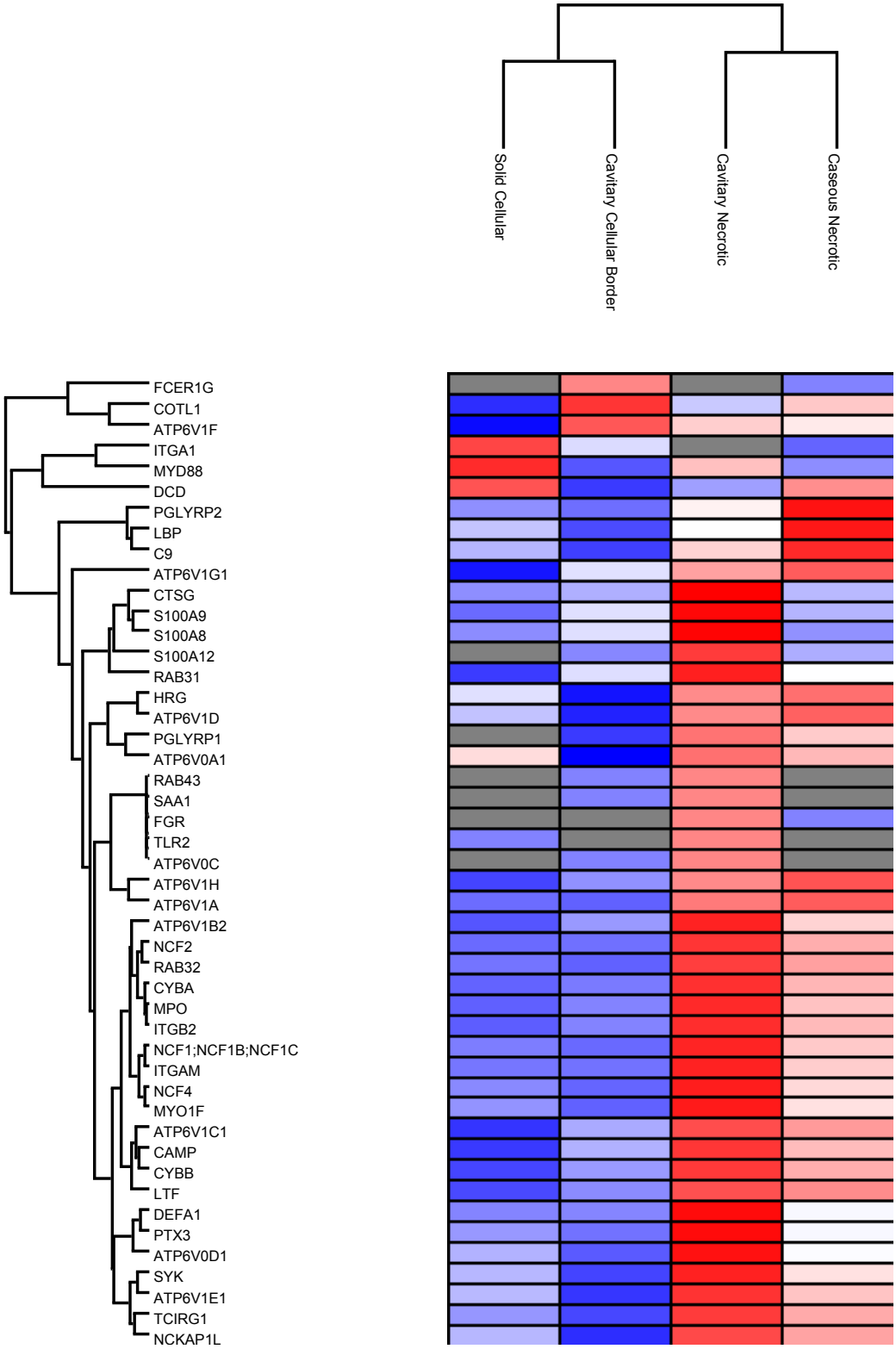

Supplemental Figure 2C

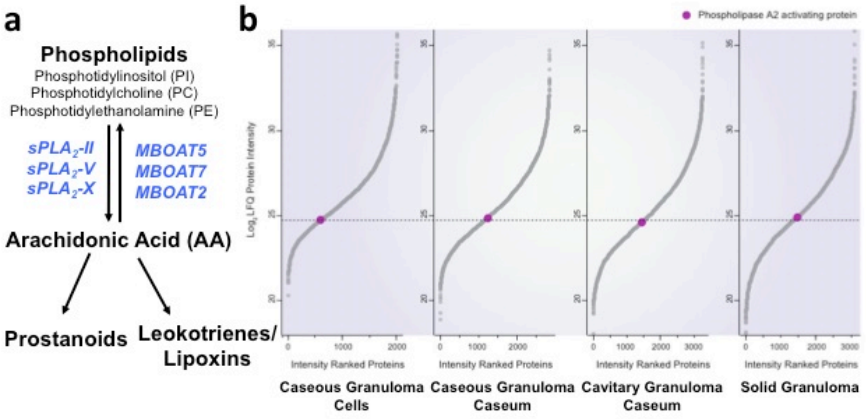

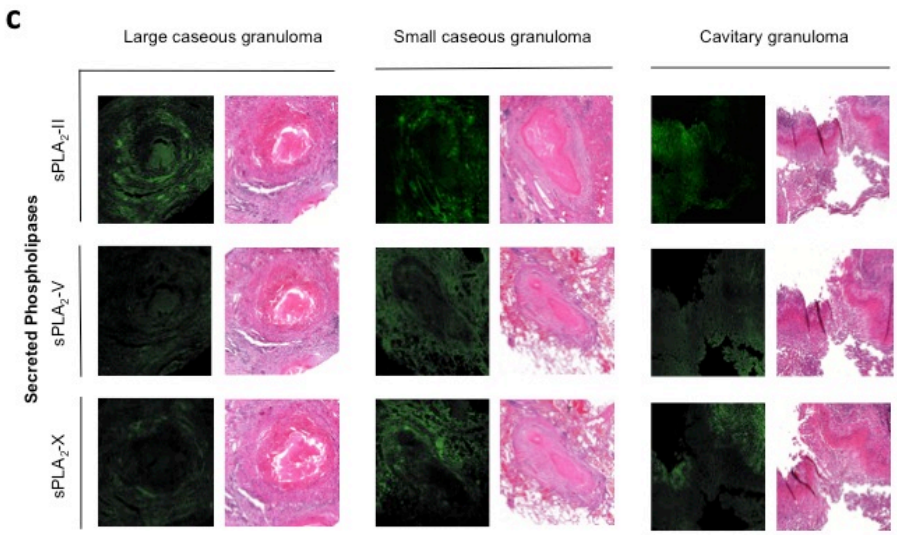

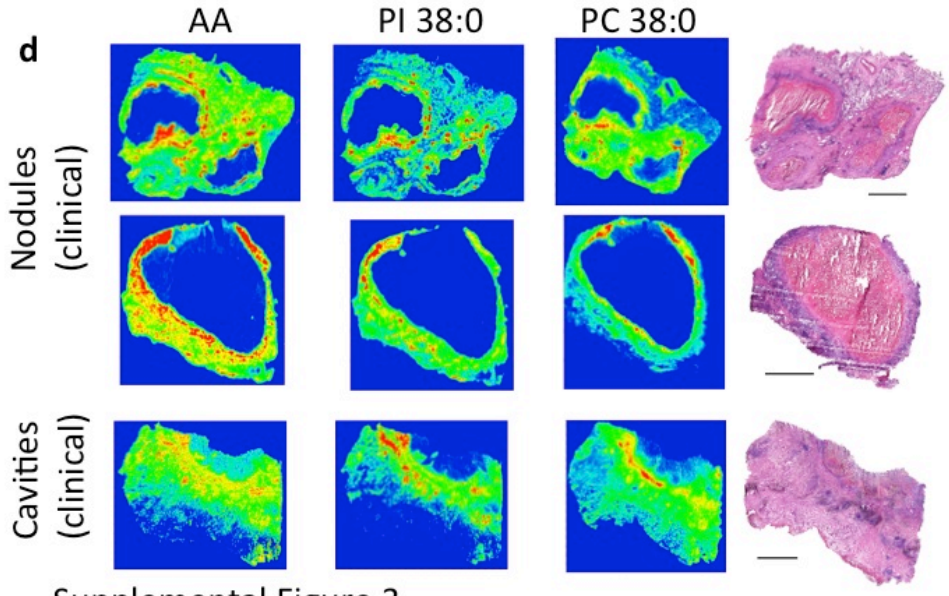

Supplemental Figure 3

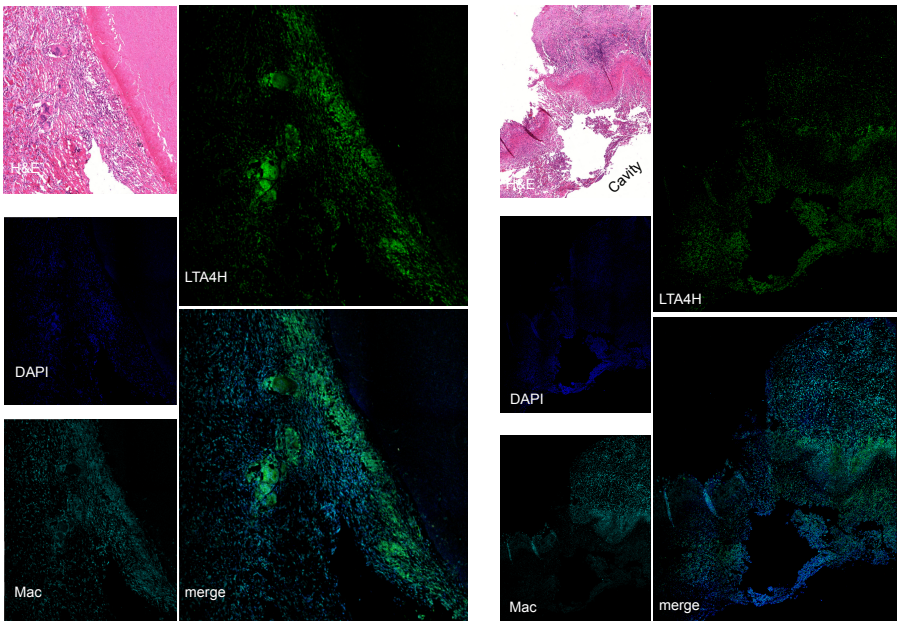

Large Caseous Granuloma Cavitary Granuloma

Supplemental Figure 4

Human Cavitary granuloma

a

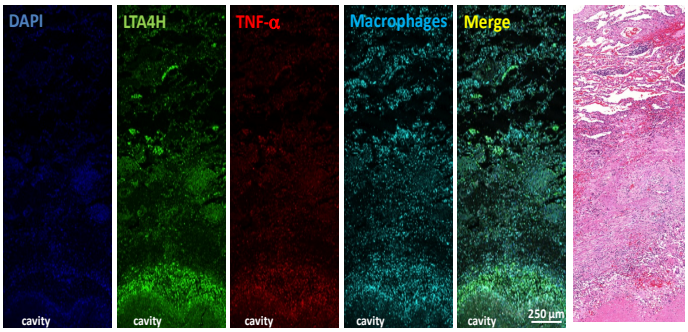

Rabbit Caseous lesion

b

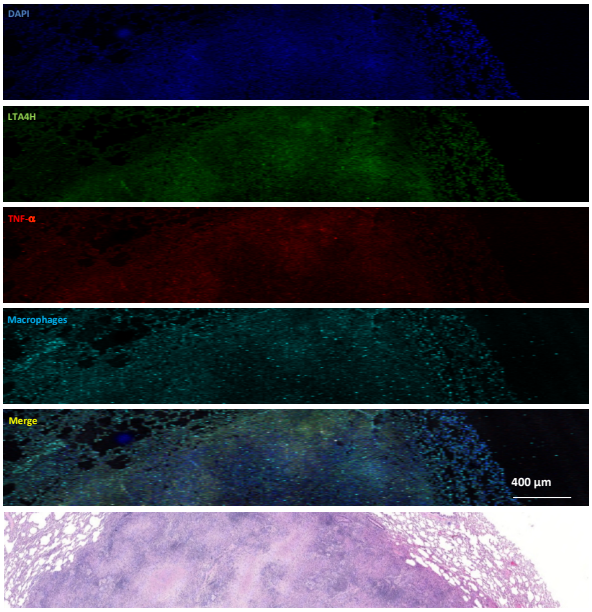

Supplemental Figure 5

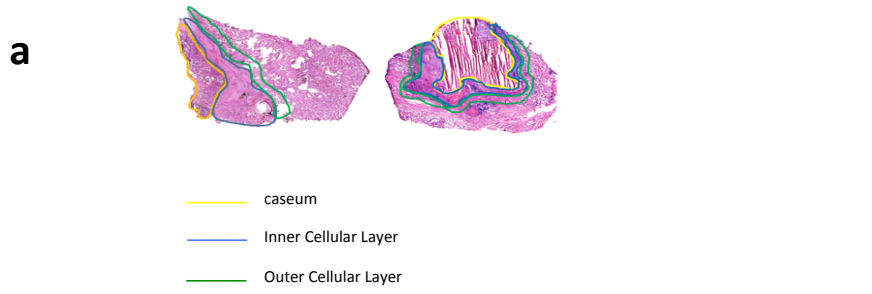

Supplemental Figure 6

Supplemental Table 1A. Summary of patients and tissue types utilized in the study

Granuloma type	Patient 070724	Patient 070327	Patient 080715	Patient 080729	Patient 070918	Patient 070619	Total samples
Cavitary	1	2	1	1	2	X	7
Caseous	X	1	2	X	1	1	5
Solid	X	1	X	X	2	1	4

Supplemental Table 1B. Samples used for Laser-Capture Microdissection and Proteomics

Patient ID:	Granuloma type	Regions dissected with LCM for Proteomics
080715	Caseous	Cellular
080715	Caseous	Caseums
070724	Cavitary	Cellular
070724	Cavitary	Caseums
070619	Solid	Cellular

Supplemental Table 1C. Details of patients and tissue samples utilized for MALDI-MSI and Immunohistochemistry (IHC)

Granuloma Type	Solid Granulomas	Caseous Granulomas	Cavitary Granulomas
Patients ID:	070619	070327	070724
Patients ID:	070327	080715	080715
Patients ID:	070918	070918	070327
Patients ID:		070619	070918
Total samples	3	4	4

Supplemental Table 1D. Details of rabbit lesions used for MALDI-MSI and IHC

Rabbit ID	Nodule (Caseous)	Cellular
2242	1	0
2245	1	1
2219	0	1
Total lesions	2	2

Supplemental Table 2: Please see the Excel file of the raw dataset of all the proteomics. The table includes imputed values as a separate sheet.

Supplemental Table 3: Please see the Excel file with PCA GO and KEGG enrichment table

Supplemental Table 4. Matrix systems used to analyze lipids in pulmonary lesion biopsies.

Matrix	Solvent system	Concentration	Ionization Mode	*m/z* Range	Lipids analyzed
CHCA	50% ACN, 0.1% TFA	5mg/mL	Positive	450-900	PC, LPC, SM
9-AA	50% MeOH	10mg/mL	Negative	500-900	PI, PE
9-AA	50% MeOH	10mg/mL	Negative	100-500	FFA

All matrices were applied to the tissue by airspray deposition. The airbrush (Paasche Model VL, Chicago, IL) was positioned at a distance of 30cm from the tissue and 20 passes over the tissue were performed with the tissue being allowed to dry for 30 seconds between coatings.

Supplemental Table 5. List of glycerophospholipid species as identified by accurate mass MALDI and MS/MS direct from tissue

Lipid Species	Ionization mode	Precursor mass (m/z)	Adduct	Identifying fragments (m/z)
LPC 16:0	Positive	518.322	$[M+Na]^+$	459 (-59)
LPC 18:0	Positive	546.353	$[M+Na]^+$	487 (-59)
LPC 18:1	Positive	544.338	$[M+Na]^+$	485 (-59)
PC 36:4	Positive	804.551	$[M+Na]^+$	745 (-59)
PC 38:4	Positive	832.582	$[M+Na]^+$	773 (-59)
PC 38:5	Positive	830.567	$[M+Na]^+$	771 (-59)
LPI 16:0	Negative	571.289	$[M-H]^-$	241
LPI 18:0	Negative	599.320	$[M-H]^-$	241, 283
LPI 18:1	Negative	597.304	$[M-H]^-$	241
PI 36:4	Negative	857.519	$[M-H]^-$	241, 303
PI 38:4	Negative	885.549	$[M-H]^-$	241, 303, 283
PI 38:5	Negative	883.534	$[M-H]^-$	241, 303
Arachidonic acid	Negative	303.233	[M-H]-	259

Supplemental Table 6: Details of antibodies used in this study

Antigen Name	Alternative Name	Host Species	Species Reactivity	Company	Catalog Number
Leukotriene A4 hydrolase	LTA4H	Rabbit	Human	Abcam	Ab109434
5 Lipoxygenase	ALOX5 or 5-LO	Rabbit	Human	Cell Signaling	3289
Cyclooxygenase 2	COX2	Rabbit	Human	Abcam	Ab15191
Cyclooxygenase 1	COX1	Mouse	Human	Abcam	Ab695
$sPLA_2$-II	sPLA2 group IIa. Phospholipase A2	Rabbit	Human	Abcam	Ab23705
$sPLA_2$-V	Secretory phospholipase A2 type V	Rabbit	Human	Acris Antibodies	APO8245PV
$sPLA_2$-X	sPLA2 group X	Rabbit monoclonal	Human	Abcam	Ab166634
Mycobacterium Tuberculosis-Biotin conjugated	MTB	Rabbit	Bacterium	Genetex	GTX36414
Iba-1	Iba-1	Goat	Human	Abcam	Ab5076
Rabbit IgG	IgG Negative	Rabbit	None	Santa Cruz	sc-2027
Goat IgG	IgG Negative	Goat	None	Santa Cruz	sc-2028
Mouse IgG1	IgG Negative	Mouse	None	Santa Cruz	sc-2025
12 lipoxygenase	ALOX-12	Rabbit	Human	Genetex	80966
Tumor Necrosis Factor Alpha	TNFα	Mouse		Abcam	Ab-1793
Iba-1		Goat		Abcam	Ab-107159
5 Lipoxygenase	ALOX-5	Goat		Santa Cruz	Sc-8885
Tumor Necrosis Factor Alpha	TNFα	Hamster		Santa Cruz	Sc-12744
Alexa 568		Hamster		Abcam	Ab-175716
MAC 387		Mouse		Abcam	Ab-22506
12 Lipoxygenase		Mouse		Ori-gene	Cf-807770